THE JOURNAL OF PHYSICAL CHEMISTRY C

Article

pubs.acs.org/JPCC

X-ray Spectroscopy of Thin Film Free-Base Corroles: A Combined Theoretical and Experimental Characterization

H. Aldahhak,[†] M. Paszkiewicz,[‡] F. Allegretti,[‡] D. A. Duncan,[‡] S. Tebi,[§] P. S. Deimel,[‡] P. Casado Aguilar,[‡] Y.-Q. Zhang,[‡] A. C. Papageorgiou,[‡] R. Koch,[§] J. V. Barth,[‡] W. G. Schmidt,[†] S. Müllegger,[§] W. Schöfberger,[∥] F. Klappenberger,*[,‡] E. Rauls,*[,†] and U. Gerstmann[†]

[†]Lehrstuhl für Theoretische Materialphysik, Universität Paderborn, 33095 Paderborn, Germany

[‡]Physik-Department E20, Technische Universität München, James-Franck-Str. 1, D-85748 Garching, Germany

[§]Institute of Semiconductor and Solid State Physics, Johannes Kepler University, Linz, Austria

[∥]Institute of Organic Chemistry, Johannes Kepler University, Linz, Austria

Supporting Information

ABSTRACT: Corrole compounds attract increasing interest due to their potential to stabilize high-valent metal states. X-ray spectroscopy is a powerful tool for the investigation and development of functional interfaces. For corrolic species, however, the required reference data are missing. Here, we employ a multitechnique X-ray investigation of thin films of the prototypical free-base 5,10,15-tris(pentafluorophenyl)-corrole (3H-TpFPC) grown on the Ag(111) surface under ultrahigh vacuum conditions. Ultrapure corrole multilayer samples are prepared and characterized by X-ray photoelectron spectroscopy (XPS) and near-edge X-ray absorption fine structure (NEXAFS) spectroscopy. In parallel, the X-ray fingerprints are simulated using the continued-fraction approach within density functional theory (DFT) for extended, (quasi-)periodic molecular structures. An excellent agreement between experimental and theoretical spectra enables a thorough interpretation of the detailed spectral features and proves an accurate description of the free-base corrole electronic structure within the present DFT approach. The present study provides X-ray spectroscopic references for all relevant core-level regions and absorption edges of intact molecular species and, thus, represents an ideal starting point for the comprehensive understanding of the complex chemistry of corroles in the adsorbed state toward the development of related functional interfaces.

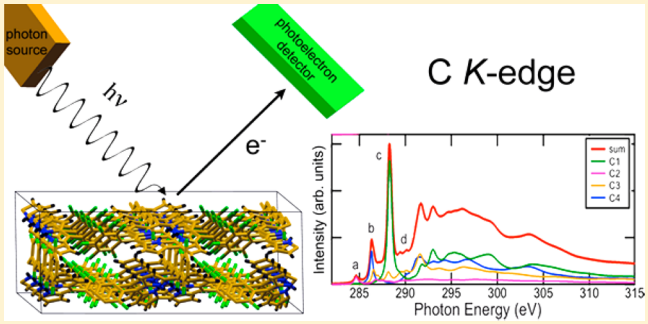

INTRODUCTION

Corroles[1,2] are structurally closely related to the well-known porphyrins that possess aromatic tetrapyrrole macrocycles. Compared to the corresponding porphyrins, they have a lower symmetry and a smaller, congested cavity.[3−5] The latter property and the resulting changes in the electronic structure promote the stabilization of metal ions in exceptionally high oxidation states.[6−8] Therefore, corroles are distinctive candidates for various biomedicine, catalysis, sensor, as well as solar cell applications.[9,10] During the past decade, extensive studies regarding the synthetic aspects[4,5,11−15] as well as the stability and activity of different corrole-chelated metal ions have been reported.[16−19] Only few studies, however, have been performed on well-defined model systems where corroles are adsorbed onto clean substrates under ultrahigh vacuum (UHV) conditions.[20−24]

Due to the minute amount of organic material involved, the determination of the geometrical structure of such interfaces by X-ray diffraction (XRD), even if utilizing surface sensitive grazing geometries (surface XRD), is prohibitively difficult; it is further hindered by the inability to grow large, ordered domains sufficient to allow such a study. However, interfaces and thin films can be comprehensively understood at the atomic level by the combination of scanning probe techniques with X-ray spectroscopy,[25−33] i.e., X-ray photoelectron spectroscopy (XPS) and near-edge X-ray absorption fine structure (NEXAFS). Thereby density functional theory (DFT) calculations may substantially assist in the interpretation of the experimental findings.[32] For corroles, however, experimental studies based on X-ray spectroscopic methods are scarce. Also the computational simulation of the X-ray spectroscopic properties for molecules was, so far, mainly restricted to single molecular species in gas phase or in solution.[34,35] An application of DFT to predict X-ray spectra of extended, (quasi-)periodic molecular structures like crystalline molecular phases and molecular adsorbates has only recently been established.[36,37]

Received: October 1, 2016
Revised: January 4, 2017
Published: January 5, 2017

DOI: 10.1021/acs.jpcc.6b09935
J. Phys. Chem. C 2017, 121, 2192−2200

In this work, a combination of experimental and theoretical X-ray techniques is used to study condensed ultrathin films of a prototypical free-base corrole molecule, namely the 5,10,15-tris(pentafluorophenyl) corrole (3H-TpFPC, Figure 1a), on Ag(111). 3H-TpFPC is one of the most stable free-base corroles, owing to its electron-withdrawing substituents,[38] and it exhibits no structural symmetry. In particular, its liquid-phase derivatives are potential detectors for cancer cells,[39−41] while its metal complexes form efficient catalytically active species.[16,42−44] It was already subject to a number of recent studies, concerning its unique structural properties (cf. ref 11−13), its metal coordinated products [cf. ref 14, 15, and 20], as well as the formation of (sub)monolayer structures on Au(111)[23] and Ag(111).[24] In the present multitechnique X-ray study, we focus on the prototypical free-base species. After fabricating, under UHV conditions, a condensed ultrapure thin film of 3H-TpFPC on a Ag(111) surface, we obtained reference spectra of all relevant X-ray photoemission regions and absorption edges. The experimental spectra are interpreted by means of density functional theory (DFT) simulated XP and NEXAFS spectra, whereby the accurate determination of the core-level shifts (CLS) from XPS is crucial to obtain NEXAFS spectra in predictive accuracy. Analyzing the contributions of individual atoms to the total spectra allows rationalizing the detailed features of the experimental multilayer spectra. The present proof-of-principle study provides a sound basis for investigations of the corresponding (sub)monolayer structures. In fact, it can serve as a starting point for the comprehensive understanding of the still unexplored interfacial chemistry of free-base corrole molecules, for which the interaction with the substrate becomes essential.

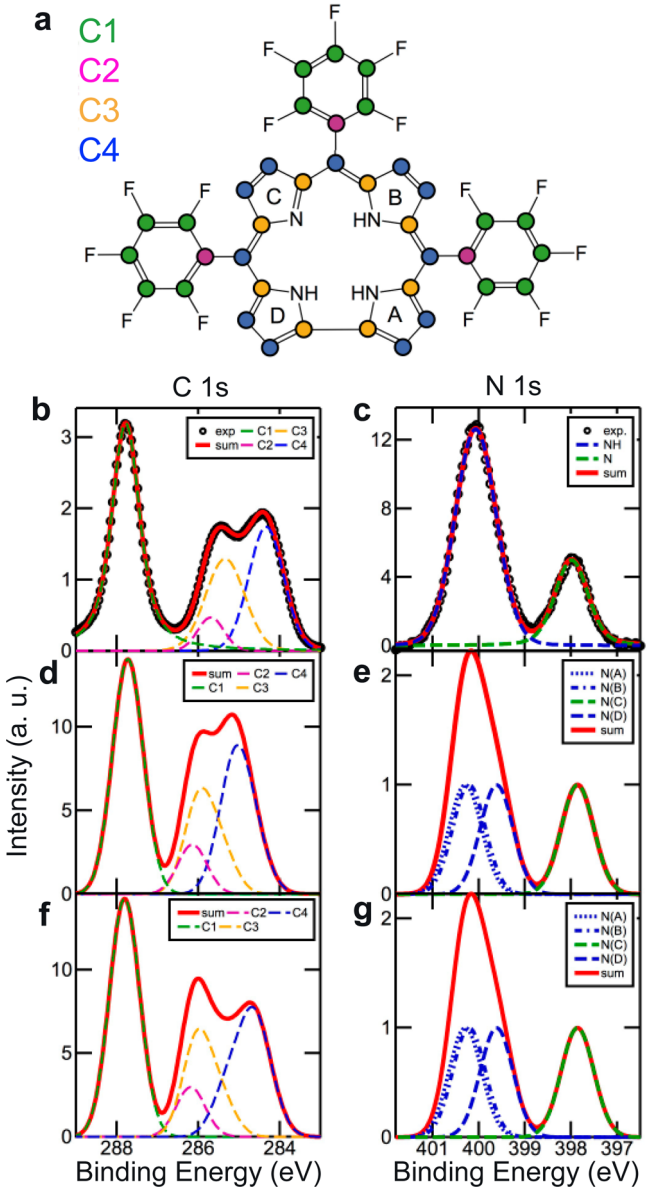

Figure 1. (a) Schematic model of free-base corrole (3H-TpFPC). Colors mark carbon atoms categorized as chemically equivalent. The letters A-D denote the chemically inequivalent pyrrole rings. Experimental XP spectra of the (b) C 1s region and (c) N 1s region of a 3H-TpFPC multilayer grown on Ag(111) compared with the corresponding simulated spectra (DFT-calculated CLS energies assuming a 0.7 eV Gaussian line width): (d and e) from gas phase modeling, (f and g) for the crystalline structure; also given: contributions of the different atom types as defined in (a).

Our paper is organized as follows: After the introduction of the experimental and theoretical methodologies, we discuss the C 1s and N 1s XP spectra of a 3H-TpFPC multilayer on Ag(111). We then present and discuss the respective K-edge NEXAFS spectra before summarizing the principal achievements in the conclusions.

METHODOLOGY

Sample Preparation. 5,10,15-Tris(pentafluorophenyl)-corrole (3H-TpFPC) was synthesized according to procedures reported in ref 14. The basic 3H-TpFPC material was purified utilizing preparative HPLC and subsequently analyzed by ^{1}H, ^{13}C and ^{19}F NMR spectroscopy. As spectroscopic quasi-periodic reference systems, we prepare 3H-TpFPC multilayer films on Ag(111) single crystals with a multilayer thickness slightly larger than 10 monolayers. The preparation and the measurements of the samples were carried out in experimental chambers with pressures in the low 10^{-9} mbar range or lower. The surface of the Ag(111) substrate (Surface Preparation Laboratory, polished to <0.5°) was cleaned by several cycles of sputtering (Ar^{+}, 1 kV) and annealing (720 K). 3H-TpFPC molecules were deposited by organic molecular beam epitaxy from a quartz crucible held at 500 K preceded with degassing in vacuo at 480 K for several hours. During the deposition of the 3H-TpFPC molecules onto the Ag(111) single crystal, the substrate was held at room temperature (300 K).

X-ray Spectroscopy. On the resulting 3H-TpFPC multilayer films XPS measurements were performed at the HE-SGM and UE56−2 PGM-2 beamlines of the BESSY II storage ring in Berlin. At the HE-SGM dipole beamline, a monochromator grating of 1500 l/mm and slit widths of 200 μm were used, together with a Scienta R3000 hemispherical analyzer with the pass energy set to 20 and 10 eV for the N/F 1s and the C 1s regions, respectively. The XPS data were recorded at room temperature (RT) and in the normal electron emission geometry.

At the UE56−2 PGM-2 undulator beamline a movable end station with a base pressure of 8×10^{-11} mbar and equipped with a SPECS Phoibos 100 CCD analyzer was used. The exit slits after the monochromator were set to 10 μm, and the entrance slits after the undulator aperture were appropriately closed to reduce the photon flux and minimize beam damage caused by the increased brilliance in comparison with the less

DOI: 10.1021/acs.jpcc.6b09935
J. Phys. Chem. C 2017, 121, 2192−2200

intense dipole magnet radiation. The sample position was also frequently changed between the acquisition of different spectra, to avoid artifacts in the XP spectra due to radiation damage. The C 1s spectra were acquired with a pass energy of 10 eV, the N 1s and F 1s at 20 eV pass energy. The photon energy, $h\nu$, was adjusted for each region such that the kinetic energy of the electrons was approximately 150 eV (C 1s 435 eV; N 1s 550 eV, F 1s 850 eV). The binding energy scale was calibrated against the Ag $3d_{5/2}$ peak (368.3 eV) after a Shirley (C 1s), linear (F 1s), or fifth-order polynomial background (N 1s) was subtracted from the raw data, and the spectra were fitted with peaks exhibiting a Voigt line shape.

Complementary NEXAFS spectra were recorded at the HE-SGM beamline with a monochromator grating of 1500 l/mm and slit widths of 200 μm in partial electron yield mode with a retarding voltage of −150 and −250 V for the C and N K-edge, respectively. The spectra were measured at different incident angles, θ, (25°, 53°, and 90°) between the electric-field vector of the incident light (90% linear polarization) and the surface normal. To improve the signal-to-noise ratio several spectra were collected and the average is presented in this work. After subtraction of the signal of the bare Ag(111) substrate from the raw data, the measured spectra were normalized to an unity edge jump.

DFT Calculations. The recorded X-ray spectra are compared to and rationalized with the help of spectra simulated from first-principles within DFT. The multilayer structure is (i) approximated by a periodic crystal structure recently determined experimentally by XRD[14] and (ii) modeled by fully relaxed molecules in the gas phase, i.e., isolated molecules in periodically repeated boxes. To optimize the microscopic structures of the investigated systems, total energy DFT calculations have been performed within the Vienna ab initio simulation package (VASP).[45] Exchange and correlation interactions have been modeled by employing the gradient-corrected PW91 functional[46] complemented with a dispersion correction (DFT-D),[47] which provides accurate adsorption energies and structures for surface-adsorbed molecules at virtually low computational costs.[48−56] The electron−ion interaction was described by pseudopotentials using the projector-augmented wave (PAW) method.[57] Plane waves with kinetic energies up to 400 eV were used as basis set. The structural relaxations were performed with convergence criteria of 0.03 eV/Å and 10^{-5} eV for forces and total energies, respectively.

For the calculation of the X-ray absorption spectra (XAS), the PAW scheme was applied in a gauge-including (GI) way: Using the Xspectra code[58,59] of the Quantum ESPRESSO package,[60] NEXAFS spectra of the C and N species were computed in a 40 eV wide energy range above the respective K-edge. The technical details like DFT-functional, dispersion correction and plane wave basis set were chosen identical to those used in the VASP total energy calculations. To model the 1s core holes, scalar-relativistic multiprojector GI-PAW pseudopotentials with a corresponding occupation of the inner shells were generated. They allow for a reliable, but computationally very efficient description of excitonic effects[61] using Lanzcos recursion scheme to expand the Green's function[62−64] (continued-fraction expansion) to be used in the calculation of the dipole and quadrupole-related XAS cross sections. This results in a particularly reliable description of near- as well as far-edge features of the absorption spectrum.[36,58,65−71] The quadrupole term is found to be negligible for the investigated systems, as it is at least 5 orders of magnitude smaller than the dipole contribution.

Due to the lack of molecular symmetry, absorption spectra need to be calculated for each atom within the molecular structure. Subsequently, the total X-ray spectrum of the molecular system is obtained from the superposition of the individual spectra offset by the corresponding CLS. The latter are calculated using a delta-scf approach, which yields highly accurate CLS for light elements such as nitrogen.[72−74] The resulting total XAS signals have been rigidly shifted to match the experimental K-edges energies. The line width is chosen energy dependent,[75] rising arctan-like from 0.2 at 395 eV (280 eV) to 2.0 at 435 eV (320 eV) for the N (C) K-edge spectra. The broadening used in the XAS calculations thus follows qualitatively the trend in the experimental spectra, but is chosen somewhat smaller, in order to prevent it from masking the spectral fine structure. The XP spectra on the other hand are obtained from a superposition of individual CLS broadened by a constant Gaussian line width of 0.7 eV as observed in experiment (cf. Figure 1).

RESULTS AND DISCUSSION

Figure 1a shows a schematic model of the investigated corrole species. 3H-TpFPC consists of a tetrapyrrolic macrocycle with three of the pyrrole moieties connected to each other via *meso*-carbon atoms and a direct C−C bond between moieties A and D. At the meso positions, three pentafluorophenyl rings are substituted. The C:F:H:N element ratio is 37:15:11:4. Strictly speaking, due to the lack of symmetry, all atoms are chemically inequivalent. However, to ease the discussion, carbon atoms with similar chemical character were grouped into four types as represented by the color coding. The positions of the H atoms within the macrocycle define two tautomeric structures T1 and T2 (Figure 2) of the macrocycle (the iminic − N= atom without H ligand placed at an inner pyrrole ring C (B) or outer

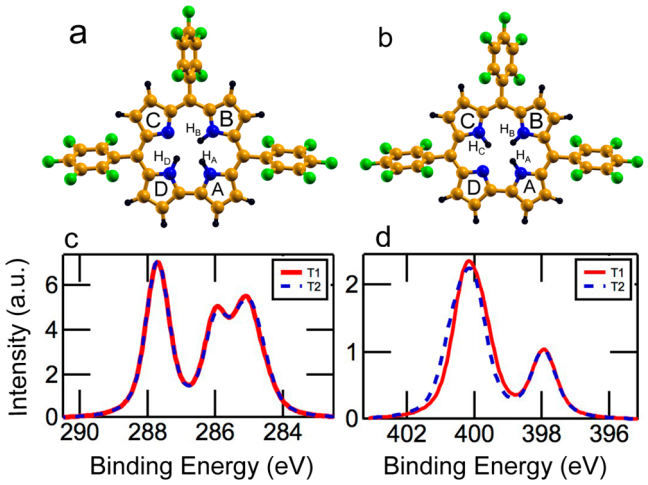

Figure 2. Ball-and-stick model of the (a) tautomer T1 and (b) tautomer T2 structures differing in the position of the iminic = N contrasting the three aminic −NH. C, N, F, and H atoms are represented in yellow, blue, green, and black, respectively. As a consequence of the steric interactions, the inner hydrogen atom H_A has been moved away (upward) from the plane, while H_B has been moved downward (T1). For tautomer T2, the up and down arrangement of the inner hydrogen atoms is inverted. (c) Calculated C 1s and (d) N 1s XP spectra for the T1 (red) and T2 (blue) tautomers.

DOI: 10.1021/acs.jpcc.6b09935
J. Phys. Chem. C 2017, 121, 2192−2200

ring D (A), respectively). Each of the two tautomers can give rise to a maximum of $2^3 \times 3^3 = 216$ conformers: $2^3 = 8$ variants are given by the orientations of the three phenyl rings (clockwise or counterclockwise); each of them provides further 3^3 variants differing in the positions of the three H atoms (in front, behind, and in-plane). However, according to our DFT total energy calculations, in the gas phase only two of these H atom configurations provide local minima: The H atom close to the iminic N atom (H_D in T1) is always found almost in-plain. Simultaneously, the remaining two H atoms (H_A and H_B) are shifted behind and in front of the plane, thereby maximizing their distance. Hence, we are left with in total 16 conformeric local minima for each tautomer.

Our and previous calculations[11] as well as the previously reported X-ray crystal structure[12] identify tautomer T1 (depicted in Figure 1a) as the dominant species. It is energetically favored by approximately 40 meV in the present calculations.

XP Spectra. The measured XP spectra of a 3H-TpFPC multilayer are presented in Figure 1b,c. The C 1s region (Figure 1b) consists of an isolated peak at a binding energy of E_B = 287.8 eV and a double peak structure with local maxima at 284.4 and 285.5 eV. The spectrum can be fitted with four components representing the four carbon types defined in Figure 1a. The relative energetic positions of these contributions can be explained by the presence of more or less electronegative elements in the vicinity of the respective carbon atoms. From higher to lower binding energy the peaks correspond to C directly connected to fluorine (C1, green, 287.8 eV), the carbon atoms of the C_6F_5 rings linked to the macrocycle (C2, purple, 285.7 eV), C with N neighbors (C3, yellow, 285.3 eV), and macrocycle C atoms without nitrogen neighbors (C4, blue, 284.3 eV), respectively. Although the C−F peak (green) exhibits a slightly higher intensity than expected, taking into account the uncertainty of the fitting procedure, the percentage area ratios of the four contributions (48:6:21:25) are in reasonable agreement with the expected ratios (15:3:8:11). We briefly note that further peaks of minor intensity can be identified for E_B > 290 eV (see also, SI Figure S1). These peaks are attributed to shakeup satellites and not further considered in this work, because they are hardly used for analyzing interfaces or thin films.

The DFT-simulated C 1s XP spectra of the molecule in gas phase are presented in Figure 1d. Since the symmetry of the molecule is broken, individual CLS for all 37 C atoms were calculated (cf. Figure S2 and Table S1). The total spectrum (red line) represents the sum over all C atoms. In addition, following the arguments given above, four contributions to the total spectrum have been determined by splitting up the C atoms according to their chemical vicinity (see also color scheme in Figure 1a). Only for the C3 group a considerable deviation from a Gaussian line shape is obtained (more evident in Figure S2). The overall shape of the total spectrum correlates very well with the experimental data, thus corroborating our assignment of the components according to the electronegativity of the neighboring atoms. The spreading of the individual carbon CLS, however, is underestimated by about 20%. This discrepancy can be partially attributed to the use of semilocal exchange-correlation functionals and an approximated description of excitonic effects,[61] but it is more likely due to an imperfect description of the experimentally investigated multilayer system by a gas phase modeling, i.e. by isolated molecules. This argument is supported by comparing the calculated XP spectrum of the gas phase shown in Figure 1d with that in Figure 1f, which corresponds to a crystalline structure (see SI, Figure S7).[14] Here, intermolecular interactions, absent for gas-phase molecules, cause a 0.3 eV outward shift of the C4 peak with respect to the rest of the spectrum ($C4_{bulk}$: 284.7 eV instead of $C4_{gas}$: 285.0 eV), resulting in a broader spectrum by 11%. An even larger broadening is expected for the experimentally investigated multilayer system, providing inhomogeneities and additional interaction with the substrate still neglected in the crystalline system.

The experimental N 1s XP spectrum of the 3H-TpFPC multilayer consists of two clearly separated peaks at 400.1 and 397.9 eV (Figure 1c). The energy position of both peaks is similar to those appearing for porphyrin species, and the relative peak areas are close to 3:1. These observations render the assignment to aminic (blue) and iminic (green) components straightforward. The simulated spectra (Figure 1e,g) based on the DFT CLS of the four nitrogen atoms perfectly agree with the experimental data and further substantiate the assignment of the components (cf. Figure S3 and Table S2). Notably, the theoretical prediction for the carbon and nitrogen XP spectra of tautomer T2 (Figure 2) can hardly be distinguished from the one presented in Figure 1d (C 1s) and 1e (N 1s). Accordingly, at least with the current state-of-the-art resolution, XPS cannot serve as a means to address tautomerism in corrole interfaces (cf. Figure S4, S5, Table S3 and S4).

NEXAFS Spectra. X-ray absorption spectroscopy is a powerful method for the analysis of molecular thin films and interfacial layers.[76−78] In particular, in the near-edge region (NEXAFS), it is sensitive to small modifications, providing valuable insight into the electronic structure,[79] conformation of flexible compounds,[80,81] interfacial charge transfer,[81,82] and chemical modifications.[83−85] The detailed knowledge of the NEXAFS signature of a suitable reference system as well as comparative theoretical data are prerequisites for a comprehensive analysis. Here, we obtained high-quality spectra of both relevant absorption edges (C and N) of a multilayer sample with the same thickness as in the XPS characterization. The measured carbon K-edge spectra are depicted in Figure 3, top panel. As to the spectral appearance, in the π^* region of the spectra (between 283 and 290 eV), we observe four well-separated maxima (A−D), whereas in the σ^* region (above 290 eV) several broad features overlap and form a continuous complex structure superimposed onto the ionization continuum. The apparent absence of dichroism suggests the presence of either a disordered arrangement of independent corrole units or small crystallites with varying orientation within the thin film. In any case, growth under the given conditions (UHV, 300 K) does not result in the formation of a well-ordered, crystalline multilayer film with molecular species aligned completely parallel (or perpendicular) to the surface plane, rendering a 1:1 theoretical modeling impossible.

The middle panel of Figure 3 displays the theoretical C K-edge NEXAFS spectrum calculated for an isolated fully relaxed 3H-TpFPC molecule. The total spectrum represents the sum of the individual absorption edges of all 37 carbon atoms. Besides the total spectrum, the contributions from the four different carbon types are also presented (thin lower lines). As remarked earlier, these contributions are already a sum over non-equivalent atoms. The overall agreement between experiment and theory is very good and the classification into the four C

DOI: 10.1021/acs.jpcc.6b09935
J. Phys. Chem. C 2017, 121, 2192−2200

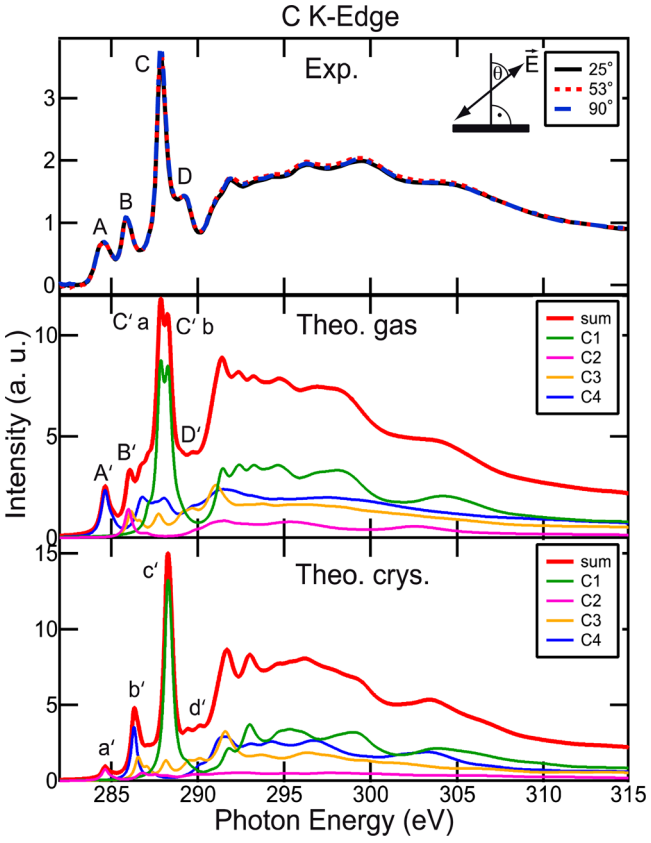

Figure 3. Experimental NEXAFS carbon K-edge spectra of a 3H-TpFPC multilayer on Ag(111) (top panel), which were measured at three photon incidence angles, θ, (25° in black, 53° in red, and 90° in blue), and comparison with the DFT calculated, angle-integrated signatures of the gas phase (middle) and crystal phase (bottom) for tautomer T1.

types allows a meaningful interpretation of the spectral features with the calculated transitions. The first resonance A′ results from excitations from C4 atoms (blue line) into the lowest macrocyclic π^* orbital. The second feature B′ consists of contributions from C2 atoms (purple line), where electrons are excited into the lowest fluorophenyl π^* orbital, and from C3 atom transitions (yellow line) into the lowest macrocyclic π^* orbital. The following two shoulders, which are not discernible in the experiment, result from macrocyclic (blue and yellow) and fluorophenylic (green and purple) transitions, respectively. The strong C′ feature carries minor contributions from the macrocycle (blue and yellow) but is dominated by transitions from outer C1 atoms (green) into the fluorophenyl π^* orbitals. The predicted double peak structure cannot be found in the experiment, whereas the experimentally quite distinct peak D is not fully reproduced by the minor shoulder D′ in the calculated spectrum. The latter mainly contains transitions of C3 and C4 atoms into higher macrocyclic π^* orbitals. A simple explanation could be that the energy of the C'_b resonance is underestimated in the calculations, i.e., actually contributes to the experimental peak D. Again we attribute this deviation mainly to intermolecular interactions, not taken into account in the calculations for gas-phase molecules.

This argument is supported by comparing the calculated gas-phase NEXAFS spectrum (Figure 3, middle) with the spectrum (Figure 3, bottom) obtained for the crystalline structure (see also SI, Figure S7). Although the structure of the individual molecular species remains almost unchanged, for most types of carbon atoms surprisingly strong changes are observed; only the C3 component (from the inner C atoms with N neighbors) remains unchanged. Between 287 and 296 eV, considerable changes are obtained for the C1, C2 contributions of the fluorophenyl rings (green and purple lines). Thereby, the spurious splitting of the C′ peak is actually lifted. Furthermore, the separation of the c′ and b′ peaks around 287 eV becomes more evident, since here the underlying contribution of the C4-type atoms (macrocycle C atoms without nitrogen neighbors) is strongly reduced. Also the spectral shape in the high-energy regime, in particular the peak at 296 eV is now better reproduced.

Nevertheless, the intensity of the d′ component is still strongly underestimated. Presently, we attribute this remaining discrepancy to the much reduced, but still present differences between the modeled crystalline phase and the multilayer film: in particular, not to the presence of stabilizing chloroform ($CHCl_3$) counterions in the crystal phase (not included in the spectra in Figure 3, *bottom*), but to the variation of the individual molecular orientation within the thin film (neglected in the theoretical modeling).

Nardi et al.[86] published NEXAFS measurements of tetrakis (pentafluorophenyl)-porphyrin (2H-TPP(F)), a compound featuring a molecular structure closely related to 3H-TpFPC, but with a porphine macrocycle. The C K-edges of 3H-TpFPC and 2H-TPP(F) exhibit a similar shape despite the differences in the chemical structure of the macrocycle. The close similarity corroborates the conclusion of Nardi et al.[86] that for these compounds the building-block principle is valid and that fluorophenyl and macrocycle moieties constitute hardly interacting spectral signatures. Furthermore, it indicates that the contraction of the corrole macrocycle resulting from the direct pyrrole−pyrrole linking impacts on the electronic structure only to a minor extent. In line with this observation, no significant differences between the tautomers are predicted by our C K-edge XAS simulation, similar to the carbon and nitrogen XP spectra.

The situation changes considerably in case of the N K-edge XAS: In Figure 4, we analyze the experimental data (top panel) with the aid of theoretical NEXAFS spectra calculated for the gas and crystal phases (middle and bottom, respectively). Again, the experimental spectra exhibit only negligible dichroism with varying incidence angle, θ largely confirming our conclusion of the absence of orientational order in the thin film already drawn from the C K-edge. Several peaks are distinguishable, four of them (E−H at 397.9, 400.3, 402.1, and 403.1 eV, respectively) situated in the π^* region and one in the σ^* region (I at 406.6 eV). In the residual part of the σ^* region (energies larger than 410 eV), a continuous, broad feature is present.

Already the calculated gas phase absorption edge (Figure 4, middle panel, red solid line) of tautomer T1 reproduces the major features and the overall shape of the experimental spectra with a reasonably good agreement for a wide energy range up to 30 eV above the edge. In the σ^* region, the theoretical spectrum contains peaks with a clearer definition as compared to the smeared out character in the experimental spectra. Hence, we attribute the absence of discernible features in the experimental spectra to statistical broadening introduced by multilayer anisotropies. The deconvolution of the spectrum into the contributions from the four distinct N atoms (thin lower lines) allows assigning the individual features. Peak E′

DOI: 10.1021/acs.jpcc.6b09935
J. Phys. Chem. C 2017, 121, 2192−2200

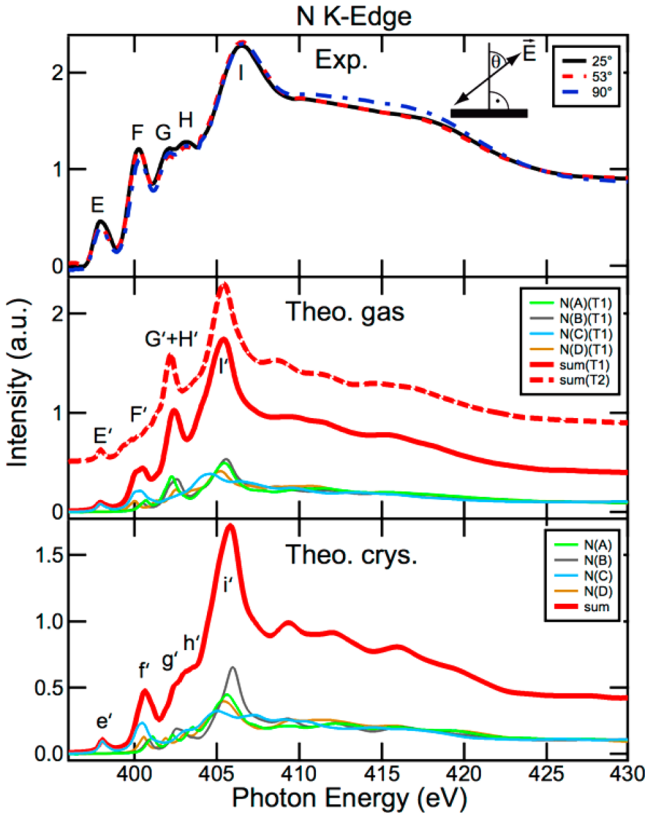

Figure 4. Comparison of experimental NEXAFS N K-edge spectra (top) of a multilayer of 3H-TpFPC on Ag (111) measured for three incidence angles, θ, (25° in black, 53° in red, and 90° in blue) with the theoretical gas-phase signatures calculated for tautomers T1, T2 (middle) and crystal phase (T1, bottom). For the DFT calculated, angular averaged spectra, the contributions from the four nitrogen atoms (A–D, cf. Figure 1) are also presented.

results solely from the N 1s → LUMO transition of the iminic N_C atom (blue line). Feature F′, which appears as a single peak in the experimental data, combines contributions from transitions of N_C to higher π^* molecular orbitals of the macrocycle and transitions of the three aminic nitrogens (green, gray, brown lines) into the LUMO. Thus, the energy splitting of the E and F peaks in the experimental spectrum (397.9 vs 400.3 eV) reflects the difference between the binding energy of the aminic and iminic N 1s core levels (2.2 eV). The next feature exhibits a single maximum at 402.4 eV but is denoted as G′+H′, since it relates to the two experimental peaks G and H. This feature is a combination of transitions of all N atoms into higher-lying π^* orbitals. The resonance I consists of contributions from σ^* resonances related to the N–C bonds of the three aminic N atoms (green, gray, and brown lines) with a leading shoulder resulting from N_C σ^* resonances. Interestingly, the characteristic peak F′ is nearly completely suppressed for tautomer T2 (middle panel, red dashed line), indicating that tautomer T1 is the highly dominant species in the multilayer sample. This global picture is further corroborated by analyzing the influence of intermolecular interactions within the crystal phase onto the shape of the nitrogen absorption edge.

The comparison of the crystal phase spectra (Figure 4, bottom panel) with those from tautomer T1 in the gas phase (middle panel) reveals minor changes for F′, E′, I′, and the higher σ^* range, but significant impact on feature G′+H′. It is now split into a series of shoulders (one for g′ and two for h′) originating from a downshift of N_B transitions and a splitting of N_A transitions. This restructuring also produces the sharpened appearance of feature f′ thereby improving the similarity to the experimental data significantly. In this respect, the N K-edge signature unfolds an intriguing sensitivity to the noncovalent, and thus weak, intermolecular interactions present in the thin film samples. Such spectroscopic sensitivity combined with the meaningful interpretation achieved by the precise modeling emphasizes the potential of our approach for the analysis of more complex functional interfaces. Furthermore, our findings reveal that in UHV grown multilayer films tautomer T1 is the largely dominating species in full accordance with earlier reports on crystals obtained by evaporation from ethyl acetate which also consisted of well-defined tautomers.[12]

CONCLUSIONS

Our combined approach of high-resolution X-ray spectroscopy assisted by DFT simulations gives access to the properties of condensed corrole multilayer thin films and provides unprecedented insight into the complex molecular structure of prototypical free-base corroles. Importantly, the overall shape of the simulated crystal phase XAS reproduces the experimental data to a level surpassing previous investigations: In the raising edge it achieves description of similar quality as usually obtained with more expensive time-dependent DFT methods,[86−89] which are typically restricted to gas-phase (single molecule) calculations. In the NEXAFS regime the use of periodic boundary conditions, a plane wave basis set, and multiprojector pseudopotentials allows for a reasonable description of scattering into delocalized unbound states in a wide energy range up to 30 eV and more above the edge. Characteristic features resulting from small variations of the electronic and atomic structure can be resolved, e.g., discrimination between slightly different structures (tautomers) and environments (gas phase or crystalline phase) can be achieved. Our results demonstrate a high sensitivity toward intermolecular interactions and the necessity to include those in the modeling. We identified that the molecular species remain intact and appear in a single tautomer (with the iminic N at an inner pyrrolic ring) in the partially disordered thin film investigated here. The computational approach applied here can be straightforwardly extended to more complex architectures including the treatment of molecular adsorbates on solid surfaces.

ASSOCIATED CONTENT

Supporting Information

The Supporting Information is available free of charge on the ACS Publications website at DOI: 10.1021/acs.jpcc.6b09935.

Measured C 1s XP spectrum of the 3H-TpFPC showing the shakeup signal, additional (measured and calculated); XP spectra of the F 1s region; DFT-calculated CLS for each C and N atom in tautomers T1 and T2 and respective simulated spectra; crystal structure of 3H-TpFPC used in the DFT modeling. (PDF)

AUTHOR INFORMATION

Corresponding Authors

*E-mail: florian.klappenberger@tum.de.
*E-mail: eva.rauls@uni-paderborn.de,.

DOI: 10.1021/acs.jpcc.6b09935
J. Phys. Chem. C 2017, 121, 2192−2200

ORCID

F. Klappenberger: 0000-0002-2877-6105

Notes

The authors declare no competing financial interest.

■ ACKNOWLEDGMENTS

This work was made possible via FWF D-A-CH i958. Further funding provided by the European Union via ERC Advanced Grant MolArt (Grant 247299), the German Research Foundation (DFG) via KL 2294/3-1, FOR 1405, and GRK 1464, the Munich-Centre for Advanced Photonics (MAP), and the Austrian Science Fund (FWF-P28167), is gratefully acknowledged. Computational resources were allocated at the Paderborn Center for Parallel Computing (PC^2). We also thank the Helmholtz-Zentrum Berlin for the allocation of synchrotron radiation beamtime and for financial support.

■ REFERENCES

(1) Gross, Z.; Galili, N. N-Substituted corroles: a novel class of chiral ligands. *Angew. Chem., Int. Ed.* **1999**, *38*, 2366−2369.

(2) Paolesse, R.; Mini, S.; Sagone, F.; Boschi, T.; Jaquinod, L.; Nurco, D. J.; Smith, K. M. 5,10,15-triphenylcorrole: a product from a modified Rothemund reaction. *Chem. Commun.* **1999**, 1307−1308.

(3) Meier-Callahan, A. E.; Gray, H. B.; Gross, Z. Stabilization of high-valent metals by corroles: oxo[tris(pentafluorophenyl) corrolato]-chromium(V). *Inorg. Chem.* **2000**, *39*, 3605−3607.

(4) Gryko, D. T.; Koszarna, B. Refined methods for the synthesis of meso-substituted A_3- and trans-A_2B-corroles. *Org. Biomol. Chem.* **2003**, *1*, 350−357.

(5) Balazs, Y. S.; Saltsman, I.; Mahammed, A.; Tkachenko, E.; Golubkov, G.; Levine, J.; Gross, Z. High-resolution NMR spectroscopic trends and assignment rules of metal-free, metallated and substituted corroles. *Magn. Reson. Chem.* **2004**, *42*, 624−635.

(6) Aviv, I.; Gross, Z. Corrole-based applications. *Chem. Commun.* **2007**, 1987−1999.

(7) Aviv-Harel, I.; Gross, Z. Aura of corroles. *Chem. - Eur. J.* **2009**, *15*, 8382−8394.

(8) Mahammed, A.; Gross, Z. Highly efficient catalase activity of metallocorroles. *Chem. Commun.* **2010**, *46*, 7040−7042.

(9) Radecki, J.; Stenka, I.; Dolusic, E.; Dehaen, W. Corroles as receptors in liquid membrane electrodes and their potentiometric response towards salicylic acid. *Electrochim. Acta* **2006**, *51*, 2282−2288.

(10) Walker, D.; Chappel, S.; Mahammed, A.; Brunschwig, B. S.; Winkler, J. R.; Gray, H. B.; Zaban, A.; Gross, Z. Corroles-sensitized TiO_2 solar cells. *J. Porphyrins Phthalocyanines* **2006**, *10*, 1259−1262.

(11) Capar, J.; Conradie, J.; Beavers, C. M.; Ghosh, A. Molecular structures of free-base corroles: nonplanarity, chirality, and enantiomerization. *J. Phys. Chem. A* **2015**, *119*, 3452−3457.

(12) Ding, T.; Harvey, J. D.; Ziegler, C. J. N-H tautomerization in triaryl corroles. *J. Porphyrins Phthalocyanines* **2005**, *9*, 22−27.

(13) Gross, Z.; Galili, N.; Simkhovich, L.; Saltsman, I.; Botoshansky, M.; Bläser, D.; Boese, D.; Goldberg, I. Solvent-free condensation of pyrrole and pentafluorobenzaldehyde: a novel synthetic pathway to corrole and oligopyrromethenes. *Org. Lett.* **1999**, *1*, 599−602.

(14) Reith, L. M.; Stiftinger, M.; Monkowius, U.; Knör, G.; Schöfberger, W. Synthesis and characterization of a stable bismuth(III) A3−corrole. *Inorg. Chem.* **2011**, *50*, 6788−6797.

(15) Schöfberger, W.; Faschinger, F.; Chattopadhyay, S.; Bhakta, S.; Mondal, B.; Elemans, J. A. A. W.; Müllegger, S.; Tebi, S.; Koch, R.; Klappenberger, F.; et al. A bifunctional electrocatalyst for oxygen evolution and oxygen reduction reactions in water. *Angew. Chem., Int. Ed.* **2016**, *55*, 2350−2355.

(16) Golubkov, G.; Bendix, J.; Gray, H. B.; Mahammed, A.; Goldberg, I.; DiBilio, A. J.; Gross, Z. High-valent manganese corroles and the first perhalogenated metallocorrole catalyst. *Angew. Chem.* **2001**, *113*, 2190−2192.

(17) Licoccia, S.; Paolesse, R.; Tassoni, E.; Polizio, F.; Boschi, T. First-row transition-metal complexes of corroles: synthesis and characterization of oxotitanium(IV) and oxovanadium(IV) complexes of β-alkylcorroles. *J. Chem. Soc., Dalton Trans.* **1995**, 3617−3621.

(18) Saltsman, I.; Balazs, Y.; Goldberg, I.; Gross, Z. Synthesis, spectroscopy, and structures of chiral rhodium(I) corrole complexes. *J. Mol. Catal. A: Chem.* **2006**, *251*, 263−269.

(19) Thomas, K. E.; Wasbotten, I. H.; Ghosh, A. Copper β-octakis(trifluoromethyl)corroles: new paradigms for ligand substituent effects in transition metal complexes. *Inorg. Chem.* **2008**, *47*, 10469−10478.

(20) Kuck, S.; Hoffmann, G.; Bröring, M.; Fechtel, M.; Funk, M.; Wiesendanger, R. Naked" iron-5,10,15-triphenylcorrole on Cu(111): observation of chirality on a surface and manipulation of multiple conformational states by STM. *J. Am. Chem. Soc.* **2008**, *130*, 14072−14073.

(21) Miao, X.; Gao, A.; Hiroto, S.; Shinokubo, H.; Osuka, A.; Xin, J.; Deng, W. Adsorption characteristic of self-assembled corrole dimers on HOPG. *Surf. Interface Anal.* **2009**, *41*, 225−230.

(22) Kuck, S.; Prostak, M.; Funk, M.; Bröring, M.; Hoffmann, G.; Wiesendanger, R. Disposition of the axial ligand in the physical vapor deposition of organometallic complexes. *J. Vac. Sci. Technol., A* **2010**, *28*, 795−798.

(23) Rashidi, M.; Müllegger, S.; Roithner, M.; Schöfberger, W.; Koch, R. Spectroscopic scanning tunneling microscopy studies of single surface-supported free-base corroles. *J. Am. Chem. Soc.* **2012**, *134*, 91−94.

(24) Tebi, S.; Aldahhak, H.; Serrano, G.; Schöfberger, W.; Rauls, E.; Schmidt, W. G.; Koch, R.; Müllegger, S. Manipulation resolves non-trivial structure of corrole monolayer on Ag(111). *Nanotechnology* **2016**, *27*, 025704−025708.

(25) Wäckerlin, C.; Chylarecka, D.; Kleibert, A.; Müller, K.; Iacovita, C.; Nolting, F.; Jung, T. A.; Ballav, N. Controlling spins in adsorbed molecules by a chemical switch. *Nat. Commun.* **2010**, *1*, 61−67.

(26) Hieringer, W.; Flechtner, K.; Kretschmann, A.; Seufert, K.; Auwärter, W.; Barth, J. V.; Görling, A.; Steinrück, H. P.; Gottfried, J. M. The surface trans effect: influence of axial ligands on the surface chemical bonds of adsorbed metalloporphyrins. *J. Am. Chem. Soc.* **2011**, *133*, 6206−6222.

(27) Duncan, D. A.; Deimel, P. S.; Wiengarten, A.; Han, R.; Acres, R. G.; Auwärter, W.; Feulner, P.; Papageorgiou, A. C.; Allegretti, F.; Barth, J. V. Immobilised molecular catalysts and the role of the supporting metal substrate. *Chem. Commun.* **2015**, *51*, 9483−9486.

(28) Diller, K.; Klappenberger, F.; Allegretti, F.; Papageorgiou, A. C.; Fischer, S.; Wiengarten, A.; Joshi, S.; Seufert, K.; Écija, D.; Auwärter, W.; et al. Investigating the molecule-substrate interaction of prototypic tetrapyrrole compounds: adsorption and self-metalation of porphine on Cu(111). *J. Chem. Phys.* **2013**, *138*, 154710.

(29) Buchner, F.; Flechtner, K.; Bai, Y.; Zillner, E.; Kellner, I.; Steinrück, H. P.; Marbach, H.; Gottfried, J. M. Coordination of iron atoms by tetraphenylporphyrin monolayers and multilayers on Ag(111) and formation of iron-tetraphenylporphyrin. *J. Phys. Chem. C* **2008**, *112*, 15458−15465.

(30) Xiao, J.; Ditze, S.; Chen, M.; Buchner, F.; Stark, M.; Drost, M.; Steinrück, H. P.; Gottfried, J. M.; Marbach, H. Temperature-dependent chemical and structural transformations from 2H-tetraphenylporphyrin to copper(II)-tetraphenylporphyrin on Cu(111). *J. Phys. Chem. C* **2012**, *116*, 12275−12282.

(31) Klappenberger, F.; Kühne, D.; Marschall, M.; Neppl, S.; Krenner, W.; Nefedov, A.; Strunskus, T.; Fink, K.; Wöll, C.; Klyatskaya, S.; et al. Uniform π-system alignment in thin films of template-grown dicarbonitrile-oligophenyls. *Adv. Funct. Mater.* **2011**, *21*, 1631−1642.

(32) Klappenberger, F. Two-dimensional functional molecular nanoarchitectures − complementary investigations with scanning tunneling microscopy and X-ray spectroscopy. *Prog. Surf. Sci.* **2014**, *89*, 1−55.

(33) Diller, K.; Klappenberger, F.; Marschall, M.; Hermann, K.; Nefedov, A.; Wöll, C.; Barth, J. V. Self-metalation of 2H-

DOI: 10.1021/acs.jpcc.6b09935
J. Phys. Chem. C 2017, 121, 2192−2200

tetraphenylporphyrin on Cu(111): an X-ray spectroscopy study. *J. Chem. Phys.* **2012**, *136*, 014705.
(34) Shimada, H.; Fukao, T.; Minami, H.; Ukai, M.; Fujii, K.; Yokoya, A.; Fukuda, Y.; Saitoh, Y. Nitrogen K-edge X-ray absorption near edge structure (XANES) spectra of purine-containing nucleotides in aqueous solution. *J. Chem. Phys.* **2014**, *141*, 055102.
(35) Shimada, H.; Minami, H.; Okuizumi, N.; Sakuma, I.; Ukai, M.; Fujii, K.; Yokoya, A.; Fukuda, Y.; Saitoh, Y. Nitrogen K-edge X-ray absorption near edge structure of pyrimidine-containing nucleotides in aqueous solution. *J. Chem. Phys.* **2015**, *142*, 175102.
(36) Vollmers, N. J.; Müller, P.; Hoffmann, A.; Herres-Pawlis, S.; Rohrmüller, M.; Schmidt, W. G.; Gerstmann, U.; Bauer, M. Experimental and theoretical high-energy-resolution X-ray absorption spectroscopy: implications for the investigation of the entatic state. *Inorg. Chem.* **2016**, *55*, 11694−11706.
(37) Baby, A.; Lin, H.; Brivio, G. P.; Floreano, L.; Fratesi, G. Core-level spectra and molecular deformation in adsorption: V-shaped pentacene on Al(001). *Beilstein J. Nanotechnol.* **2015**, *6*, 2242−2251.
(38) Geier, G. R.; Chick, J. F. B.; Callinan, J. B.; Reid, C. G.; Auguscinski, W. P. A survey of acid catalysis and oxidation conditions in the two-step, one-flask synthesis of meso-substituted corroles via dipyrromethanedicarbinols and pyrrole. *J. Org. Chem.* **2004**, *69*, 4159−4169.
(39) Aviezer, D.; Cotton, S.; David, M.; Segev, A.; Khaselev, N.; Galili, N.; Gross, Z.; Yayon, A. Porphyrin analogues as novel antagonists of fibroblast growth factor and vascular endothelial growth factor receptor binding that inhibit endothelial cell proliferation, tumor progression, and metastasis. *Cancer Res.* **2000**, *60*, 2973−2980.
(40) Bendix, J.; Dmochowski, I. J.; Gray, H. B.; Mahammed, A.; Simkhovich, L.; Gross, Z. Structural, electrochemical, and photophysical properties of gallium(III) 5,10,15-tris (pentafluorophenyl)-corrole. *Angew. Chem., Int. Ed.* **2000**, *39*, 4048−4051.
(41) Mahammed, A.; Gross, Z. Aluminum corrolin, a novel chlorophyll analogue. *J. Inorg. Biochem.* **2002**, *88*, 305−309.
(42) Gross, Z.; Simkhovich, L.; Galili, N. First catalysis by corrole metal complexes: epoxidation, hydroxylation, and cyclopropanation. *Chem. Commun.* **1999**, 599−600.
(43) Gross, Z.; Golubkov, G.; Simkhovich, L. Epoxidation catalysis by a manganese(III) corrole and isolation of an oxomanganese(V) corrole. *Angew. Chem., Int. Ed.* **2000**, *39*, 4045−4047.
(44) Simkhovich, L.; Mahammed, A.; Goldberg, I.; Gross, Z. Synthesis and characterization of germanium, tin, phosphorous, iron, and rhodium complexes of tris(pentafluorophenyl)corrole, and the utilization of the iron and rhodium corroles as cyclopropanation catalysts. *Chem. - Eur. J.* **2001**, *7*, 1041−1055.
(45) Kresse, G.; Furthmüller, J. Efficiency of ab-initio total energy calculations for metals and semiconductors using a plane-wave basis set. *Comput. Mater. Sci.* **1996**, *6*, 15−50.
(46) Perdew, J. P.; Chevary, J. A.; Vosko, S. H.; Jackson, K. A.; Pederson, M. R.; Singh, D. J.; Fiolhais, C. Atoms, molecules, solids, and surfaces: applications of the generalized gradient approximation for exchange and correlation. *Phys. Rev. B: Condens. Matter Mater. Phys.* **1992**, *46*, 6671−6687.
(47) Ortmann, F.; Bechstedt, F.; Schmidt, W. G. Semiempirical van der Waals correction to the density functional description of solids and molecular structures. *Phys. Rev. B: Condens. Matter Mater. Phys.* **2006**, *73*, 05101.
(48) Guo, Q.; Paulheim, A.; Sokolowski, M.; Aldahhak, H.; Rauls, E.; Schmidt, W. G. Adsorption of PTCDA on terraces and at steps sites of the KCl(100) surface. *J. Phys. Chem. C* **2014**, *118*, 29911−29918.
(49) Aldahhak, H.; Matencio, S.; Barrena, E.; Ocal, C.; Schmidt, W. G.; Rauls, E. Structure formation in diindenoperylene thin films on copper(111). *Phys. Chem. Chem. Phys.* **2015**, *17*, 8776−8783.
(50) McNellis, E. R.; Meyer, J.; Reuter, K. Azobenzene at coinage metal surfaces: role of dispersive van der Waals interactions. *Phys. Rev. B: Condens. Matter Mater. Phys.* **2009**, *80*, 205414−10.
(51) Aldahhak, H.; Rauls, E.; Schmidt, W. G. Diindenoperylene adsorption on Cu(111) studied with density-functional theory. *Surf. Sci.* **2015**, *641*, 260−265.
(52) Aldahhak, H.; Schmidt, W. G.; Rauls, E. Adsorption of PTCDA on NaCl(100) and KCl(100). *Surf. Sci.* **2013**, *617*, 242−248.
(53) Aldahhak, H.; Schmidt, W. G.; Rauls, E. Single PTCDA molecules on planar and stepped KCl and NaCl (100) surfaces. *Surf. Sci.* **2015**, *641*, 278−281.
(54) Thierfelder, C.; Witte, M.; Blankenburg, S.; Rauls, E.; Schmidt, W. G. Methane adsorption on graphene from first principles including dispersion interaction. *Surf. Sci.* **2011**, *605*, 746−749.
(55) Paulheim, A.; Marquardt, C.; Aldahhak, H.; Rauls, E.; Schmidt, W. G.; Sokolowski, M. Inhomogeneous and homogeneous line broadening of optical spectra of PTCDA molecules adsorbed at step edges of alkali halide surfaces. *J. Phys. Chem. C* **2016**, *120*, 11926−11937.
(56) Paulheim, A.; Marquardt, C.; Sokolowski, M.; Hochheim, M.; Bredow, T.; Aldahhak, H.; Rauls, E.; Schmidt, W. G. Surface induced vibrational modes in the fluorescence spectra of PTCDA adsorbed on the KCl(100) and NaCl(100) surfaces. *Phys. Chem. Chem. Phys.* **2016**, *18*, 32891−32902.
(57) Kresse, G.; Joubert, D. From ultrasoft pseudopotentials to the projector augmented-wave method. *Phys. Rev. B: Condens. Matter Mater. Phys.* **1999**, *59*, 1758−1775.
(58) Taillefumier, M.; Cabaret, D.; Flank, A. M.; Mauri, F. X-ray absorption near-edge structure calculations with the pseudopotentials: application to the K edge in diamond and α-quartz. *Phys. Rev. B: Condens. Matter Mater. Phys.* **2002**, *66*, 195107.
(59) Gougoussis, C.; Calandra, M.; Seitsonen, A. P.; Mauri, F. First-principles calculations of X-ray absorption in a scheme based on ultrasoft pseudopotentials: from α-quartz to high-Tc compounds. *Phys. Rev. B: Condens. Matter Mater. Phys.* **2009**, *80*, 075102.
(60) Giannozzi, P.; Baroni, S.; Bonini, N.; Calandra, M.; Car, R.; Cavazzoni, C.; Ceresoli, D.; Chiarotti, G. L.; Cococcioni, M.; Dabo, I.; et al. QUANTUM ESPRESSO: a modular and open-source software project for quantum simulations of materials. *J. Phys.: Condens. Matter* **2009**, *21*, 395502−395520.
(61) Buczko, R.; Duscher, G.; Pennycook, S. J.; Pantelides, S. T. Excitonic effects in core-excitation spectra of semiconductors. *Phys. Rev. Lett.* **2000**, *85*, 2168−2171.
(62) Lanczos, C.; Res, J. Solution of systems of linear equations by minimized iterations. *Natl. Bur. Stand.* **1952**, *49*, 33−53.
(63) Haydock, R.; Heine, V.; Kelly, M. J. Electronic structure based on the local atomic environment for tight-binding bands. II. *J. Phys. C: Solid State Phys.* **1975**, *8*, 2591−2605.
(64) Walker, B.; Gebauer, R. Ultrasoft pseudopotentials in time-dependent density-functional theory. *J. Chem. Phys.* **2007**, *127*, 164106.
(65) Gaudry, E.; Cabaret, D.; Brouder, C.; Letard, I.; Rogalev, A.; Wilhlem, F.; Jaouen, N.; Sainctavit, P. Relaxations around the substitutional chromium site in emerald: X-ray absorption experiments and density functional calculations. *Phys. Rev. B: Condens. Matter Mater. Phys.* **2007**, *76*, 094110.
(66) Juhin, A.; Brouder, C.; Arrio, M. A.; Cabaret, D.; Sainctavit, P.; Balan, E.; Bordage, A.; Seitsonen, A. P.; Calas, G.; Eeckhout, S. G.; et al. X-ray linear dichroism in cubic compounds: the case of Cr^{3+} in $MgAl_2O_4$. *Phys. Rev. B: Condens. Matter Mater. Phys.* **2008**, *78*, 195103.
(67) Cabaret, D.; Mauri, F.; Henderson, G. S. Oxygen K-edge XANES of germanates investigated using first-principles calculations. *Phys. Rev. B: Condens. Matter Mater. Phys.* **2007**, *75*, 184205.
(68) Ehlert, C.; Unger, W. E. S.; Saalfrank, P. C K-edge NEXAFS spectra of graphene with physical and chemical defects: a study based on density functional theory. *Phys. Chem. Chem. Phys.* **2014**, *16*, 14083−14095.
(69) Fratesi, G.; Lanzilotto, V.; Floreano, L.; Brivio, G. P. Azimuthal dichroism in near-edge X-ray absorption Fine Structure Spectra of Planar molecules. *J. Phys. Chem. C* **2013**, *117*, 6632−6638.
(70) Fratesi, G.; Lanzilotto, V.; Stranges, S.; Alagia, M.; Brivioe, G. P.; Floreano, L. High resolution NEXAFS of perylene and PTCDI: a surface science approach to molecular orbital analysis. *Phys. Chem. Chem. Phys.* **2014**, *16*, 14834−14844.

DOI: 10.1021/acs.jpcc.6b09935
J. Phys. Chem. C 2017, 121, 2192−2200

(71) Bunău, O.; Calandra, M. Projector augmented wave calculation of X-ray absorption spectra at the L2,3 edges. *Phys. Rev. B: Condens. Matter Mater. Phys.* **2013**, *87*, 205105.
(72) Rignanese, G. M.; Pasquarello, A. Nitrogen 1s core-level shifts at the NH_3 saturated Si(100)-2 × 1 surface: a first-principles study. *Surf. Sci.* **2001**, *490*, L614−L618.
(73) Rignanese, G. M.; Pasquarello, A. Nitrogen bonding configurations at nitrided Si(001) surfaces and Si(001)-SiO_2 interfaces: a first-principles study of core-level shifts. *Phys. Rev. B: Condens. Matter Mater. Phys.* **2001**, *63*, 075307.
(74) Garcia-Gil, S.; Garcia, A.; Ordejon, P. Calculation of core level shifts within DFT using pseudopotentials and localized basis sets. *Eur. Phys. J. B* **2012**, *85*, 239.
(75) Bunău, O.; Joly, Y. Self-consistent aspects of X-ray absorption calculations. *J. Phys.: Condens. Matter* **2009**, *21*, 345501−345511.
(76) Chen, J. G. NEXAFS investigations of transition metal oxides, nitrides, carbides, sulfides and other interstitial compounds. *Surf. Sci. Rep.* **1997**, *30*, 1−152.
(77) Hähner, G. Near edge X-ray absorption fine structure spectroscopy as a tool to probe electronic and structural properties of thin organic films and liquids. *Chem. Soc. Rev.* **2006**, *35*, 1244−1255.
(78) Breuer, T.; Klues, M.; Witte, G. Characterization of orientational order in π-conjugated molecular thin films by NEXAFS. *J. Electron Spectrosc. Relat. Phenom.* **2015**, *204* (A), 102−115.
(79) Krasnikov, S. A.; Preobrajenski, A. B.; Sergeeva, N. N.; Brzhezinskaya, M. M.; Nesterov, M. A.; Cafolla, A. A.; Senge, M. O.; Vinogradov, A. S. Formation of extended covalently bonded Ni porphyrin networks on the Au(111) surface. *Chem. Phys.* **2007**, *332*, 318−324.
(80) Auwärter, W.; Klappenberger, F.; Weber-Bargioni, A.; Schiffrin, A.; Strunskus, T.; Wöll, C.; Pennec, Y.; Riemann, A.; Barth, J. V. Conformational adaptation and selective adatom capturing of tetrapyridyl-porphyrin molecules on a copper (111) surface. *J. Am. Chem. Soc.* **2007**, *129*, 11279−11285.
(81) Diller, K.; Klappenberger, F.; Marschall, M.; Hermann, K.; Nefedov, A.; Wöll, C.; Barth, J. V. Self-metalation of 2H-tetraphenylporphyrin on Cu(111): an X-ray spectroscopy study. *J. Chem. Phys.* **2012**, *136*, 014705.
(82) Bischoff, F.; Seufert, K.; Auwärter, W.; Joshi, S.; Vijayaraghavan, S.; Écija, D.; Diller, K.; Papageorgiou, A. C.; Fischer, S.; Allegretti, F.; et al. How surface bonding and repulsive interactions cause phase transformations: ordering of a prototype macrocyclic compound on Ag(111). *ACS Nano* **2013**, *7*, 3139−3149.
(83) Krasnikov, S. A.; Sergeeva, N. N.; Brzhezinskaya, M. M.; Preobrajenski, A. B.; Sergeeva, Y. N.; Vinogradov, N. A.; Cafolla, A. A.; Senge, M. O.; Vinogradov, A. S. An X-ray absorption and photoemission study of the electronic structure of Ni porphyrins and Ni N-confused porphyrin. *J. Phys.: Condens. Matter* **2008**, *20*, 235207.
(84) Di Santo, G.; Castellarin-Cudia, C.; Fanetti, M.; Taleatu, B.; Borghetti, P.; Sangaletti, L.; Floreano, L.; Magnano, E.; Bondino, F.; Goldoni, A. Conformational adaptation and electronic structure of 2H-tetraphenylporphyrin on Ag(111) during Fe metalation. *J. Phys. Chem. C* **2011**, *115*, 4155−4162.
(85) Wiengarten, A.; Seufert, K.; Auwärter, W.; Écija, D.; Diller, K.; Allegretti, F.; Bischoff, F.; Fischer, S.; Duncan, D. A.; Papageorgiou, A. C.; et al. Surface-assisted dehydrogenative homocoupling of porphine molecules. *J. Am. Chem. Soc.* **2014**, *136*, 9346−9354.
(86) Nardi, M. V.; Verucchi, R.; Pasquali, L.; Giglia, A.; Fronzoni, G.; Sambi, M.; Mangione, G.; Casarin, M. XAS of tetrakis(phenyl)- and tetrakis(pentafluorophenyl)-porphyrin: an experimental and theoretical study. *Phys. Chem. Chem. Phys.* **2015**, *17*, 2001−2011.
(87) Schmidt, N.; Fink, R.; Hieringer, W. Assignment of near-edge X-ray absorption fine structure spectra of metalloporphyrins by means of time-dependent density-functional calculations. *J. Chem. Phys.* **2010**, *133*, 054703.
(88) Besley, N. A.; Asmuruf, F. A. Time-dependent density functional theory calculations of the spectroscopy of core electrons. *Phys. Chem. Chem. Phys.* **2010**, *12*, 12024−12039.
(89) Bunău, O.; Joly, Y. Time-dependent density functional theory applied to X-ray absorption spectroscopy. *Phys. Rev. B: Condens. Matter Mater. Phys.* **2012**, *85*, 155121.

DOI: 10.1021/acs.jpcc.6b09935
J. Phys. Chem. C 2017, 121, 2192−2200